PHYSICAL REVIEW B VOLUME 44, NUMBER 10 1 SEPTEMBER 1991-II

Theory of second-harmonic generation in strongly scattering media

V. E. Kravtsov*
Physikalisches Institut der Universität Würzburg Am Hubland, 8700 Würzburg, Germany

V. M. Agranovich and K. I. Grigorishin
Institute of Spectroscopy, U.S.S.R. Academy of Sciences, 142092 Troitsk, Moscow r-n, U.S.S.R.
(Received 10 September 1990; revised manuscript received 18 March 1991)

Second-harmonic generation is studied in a medium which is both nonlinear and disordered. Disorder-induced strong elastic scattering of both a fundamental and second-harmonic light gives rise to a diffusionlike regime of light propagation. The interference effects, which cannot be described by the diffusion approximation, are taken into account. They are shown to lead to a sharp peak in the angular distribution of second-harmonic intensity. The direction of the maximum second-harmonic intensity is found to be roughly opposite to the one determined by the usual phase-matching condition in an effective transparent medium. Different models of disorder are considered, and the corresponding values of peak-to-background ratio are calculated.

I. INTRODUCTION

Recently there has been a considerable increase in the number of both experimental and theoretical works on optics of disordered media. Such a revival of the field is connected with understanding of a role played by interference effects at multiple scattering of light in absorptionless disordered media. As it has been realized, they are the effects that are responsible for the localization of waves at a sufficiently large extent of disorder (Anderson localization). However, even at weak disorder these effects are important. The most famous examples of such types are the decrease in conductivity of metals at very low temperatures[1] (weak localization) and enhanced backscattering of light from opaque media.[2–9] Recently the physical principles of weak localization have been applied to nonlinear optical phenomena.[10–11] As has been shown in Ref. 10, the same interference effects that lead to enhanced linear backscattering can produce a sharp peak in the angular distribution of second-harmonic intensity, the direction of maximum second-harmonic intensity being opposite to the one of the fundamental-light incidence. Such an effect is impossible in a transparent nonlinear medium where the second-harmonic intensity has a sharp peak in the forward direction due to the momentum-conservation law for mixing photons. It also cannot be obtained in a strongly scattering medium within the diffusion approximation, which is usually applied to this case.[12] In order to take into account the interference effects in nonlinear mixing, one should go beyond the diffusion approximation in describing the propagation of light in strongly scattering materials. The first step in this direction has been made in Ref. 10. However, in this work we have confined ourselves to the case when a medium is transparent for a fundamental light of the frequency ω and only a second-harmonic (SH) light is scattered strongly. In addition, the nonlinear polarizability $\chi^{(2)}$ is supposed to be nonrandom, constant in space value. Though the calculations are simplified considerably in this case, it does not correspond to a real experimental situation.[13]

The results of the work[13] showed that there is no problem with the registration of the output intensity of the second-harmonic radiation generated in a strongly scattering sample [pressed powder of potassium dihydrogen phosphate (KDP)]. The main experimental difficulty is the presence of an intense diffuse background, which prevented us, under the conditions available in Ref. 13, from observing the interference peak. The smallness of the peak-to-background ratio at a *stationary* second-harmonic generation in a strongly scattering bulk sample has been pointed out in Ref. 10. That is why the case of a *pulse* second-harmonic generation has been studied in Ref. 10 as a possible way to increase the relative value of the interference peak.

However, the real experimental situation is much richer than a model considered in Ref. 10. The most important phenomena, which were not taken into account in Ref. 10, are scattering of a fundamental light and disorder in the nonlinear properties of a sample. In this work a general case is studied where both a fundamental and a second-harmonic light is scattered, the elastic scattering lengths being l_ω and $l_{2\omega}$, respectively. It will be shown that in spite of fundamental-light scattering, the interference peak in the angular distribution of SH intensity is present. Moreover, fundamental-light scattering makes its observation easier because scattering suppresses the diffuse background in the angular distribution of SH intensity, and, therefore the peak-to-background ratio increases. At not too large sizes of a sample L, the maximal peak-to-background ratio is roughly equal to $l_{2\omega}/l_\omega$ in contrast to the value $l_{2\omega}/L$ found in Ref. 10 for the case $l_\omega > L$. Under real experimental conditions[13] the scattering lengths are $l_\omega \approx l_{2\omega} \approx 90$ μm, that is two orders of magnitude smaller than the sample size $L \approx 1$ cm. Thus, scattering of a fundamental light gives rise to a dramatic

increase of the peak-to-background ratio. Therefore, the predicted interference peak in the angular dependence of SH intensity could be observed even in bulk samples at stationary conditions.

However, for such experiments the choice of a sample is of great importance. The most obvious example[13] of both a nonlinear and scattering medium is a pressed powder prepared from a nonlinear crystal with nonzero $\chi^{(2)}$ (i.e., noncentrosymmetric crystal). Nevertheless, this is not an optimal (with respect to the value of the peak-to-background ratio) choice for the experiments on the interference effects in second-harmonic generation. The reason is that the average value of the nonlinear polarizability $\langle\chi^{(2)}\rangle$ [not $\langle\chi(3)\rangle$] is zero in such a medium because of its spatial isotropy.

We shall consider below both a model with a constant and a model with a random in space nonlinear polarizability. The latter model seems to be more realistic for the description of second-harmonic generation (SHG) in samples consisting of small randomly oriented particles of a nonlinear crystal. It is shown that at sufficiently small values of the particles size, $R \ll l_\omega, l_{2\omega}$, the interference peak in the SHG is smeared out. This result explains the failure[13] to observe the interference peak.

Another possible cause of this failure is connected with the phase mismatch because of the frequency dispersion of the linear dielectric constant. Although this effect has been considered in Ref. 10, it acquires different important features when fundamental-light scattering and disorder in the nonlinear constant are taken into account. In particular, it is shown in this paper that the negative frequency dispersion of the average refractive index $\Delta n = n(2\omega) - n(\omega)$ does not lead to a decrease in the second-harmonic intensity generated in a bulk scattering medium. On the contrary, the positive dispersion results in the additional suppression of the diffuse background in the second-harmonic generation. It means that the positive dispersion diminishes the peak-to-background ratio weaker than the negative one. On the other hand, if one is interested in the maximum output second-harmonic intensity, not the maximum relative value of the interference peak, the negative dispersion is preferable. Thus, a problem of optimizing the parameters of a sample appears, the solution of this problem depending on the aim of the experiment. If this aim is an observation of the interference peak, the problem reduces mainly to the optimization of the peak-to-background ratio with respect to such parameters as $l_{2\omega}/L$, $l_{2\omega}/l_\omega$, and $(l_{2\omega}/\lambda)\Delta n$, where λ is the wavelength. This problem is considered below in detail as well as the dependence of a peak shape on the parameters of a sample.

The paper is organized as follows. In Sec. II different models of disorder are described. The experimental geometry and the basic equations are given in Sec. III. In Sec. IV the impurity diagrammatic technique is generalized for the particular problem. The main results of calculations are summarized in Sec. V. The effect of the phase-matching condition is discussed in Sec. VI. Section VII is devoted to the consideration of a model with a random nonlinear polarizability. In Sec. VIII the main features of SHG in a strongly scattering medium are explained qualitatively. In the Discussion the necessary numerical estimations are made as well as some experimental recommendations on the optimal choice of samples.

II. TWO MODELS OF DISORDER

We shall consider two different models for the description of SHG in disordered materials. The first model is characterized by a nonrandom, spatially homogeneous nonlinear polarizability $\chi^{(2)}_{i,jl}$ and a random, inhomogeneous linear dielectric constant.

A possible example of a material described by this model is an absorptionless nonlinear monocrystal of the proper symmetry group (with no inversion symmetry) that contains internal scatterers (e.g., cavities). At a relatively small fraction f of volume occupied by scatterers, nonlinear properties of such a material can be described approximately by a space-averaged nonlinear polarizability. However, even weak Rayleigh scattering by internal inhomogeneities makes a sufficiently thick sample opaque due to the diffusionlike propagation of light in it.

Another example is a pressed powder of a centrosymmetric nonlinear material in a strong external electrostatic field E_0. In this case a corresponding second-order nonlinear constant $\chi^{(2)}$ is proportional to the averaged value of a third-order nonlinear constant $\chi^{(3)}$ and the value of an external electric field. In spite of the smallness of a constant $\chi^{(3)}$, such a material may be preferable to the first one because it is not easy to imbed scatterers in a single crystal.

Formally, inhomogeneous linear optical properties of a sample can be described in terms of a space-dependent dielectric tensor $\epsilon_{ij}(\mathbf{r}')$. For the sake of simplicity we restrict ourselves to the consideration of a scalar dielectric constant

$$\epsilon(\mathbf{r}) = \bar{\epsilon} + \delta\epsilon(\mathbf{r}) , \tag{2.1}$$

where the ensemble average of $\langle\delta\epsilon(\mathbf{r})\rangle$ is supposed to be zero. For the particular case when scatterers are uniformly distributed over a volume and their size a is much smaller than the wavelength of light λ, the averaged dielectric constant is given by

$$\bar{\epsilon} = \epsilon_0(1-f) + \epsilon_1 f , \tag{2.2}$$

where ϵ_0 and ϵ_1 are dielectric constants of a surround and a scatterer, respectively, and a volume fraction of scatterers f is supposed to be small. In this case a random part of the dielectric constant $\delta\epsilon(\mathbf{r})$ can be considered as a Gaussian random field characterized by a correlator:

$$\langle\delta\epsilon(\mathbf{r})\delta\epsilon(\mathbf{r}')\rangle = (\epsilon_0-\epsilon_1)^2\frac{f^2}{n}\delta(\mathbf{r}-\mathbf{r}') , \tag{2.3}$$

where n is a number of scatterers in a unit volume. The coefficient attached to the δ function in (2.3) determines an elastic scattering length l for Rayleigh scattering:

$$l^{-1} = \left[\frac{2\pi}{\lambda}\right]^4 (\epsilon_0-\epsilon_1)^2\frac{f^2}{6\pi n} . \tag{2.4}$$

Equation (2.4) shows that in the absence of frequency dispersion in the dielectric constants ϵ_0, ϵ_1 the following

relationship is valid for elastic-scattering lengths corresponding to a fundamental and a second-harmonic light:

$$l_\omega = 16 l_{2\omega} \ . \tag{2.5}$$

For short-wavelength scattering $a \gg \lambda$ the expressions (2.3)–(2.5) no longer hold. In this case one should expect the light-scattering cross section to be an independent on the wavelength value of the order of a^2. Therefore, the value $l_{2\omega}/l_\omega$ should be close to unity when $a \gg \lambda$.

The ratio $\alpha = \lambda/(2\pi l)$ plays a crucial role in the theory of light propagation through a disordered medium. For small values of α the diffusion approximation is a good zeroth-order approximation for a consideration of weak localization effects. Large value of α correspond to the strong Anderson localization of light.[14,15] For Rayleigh scattering by spherical scatterers of the radius a the parameter α is given by the expression

$$\alpha = \lambda/(2\pi l) = \frac{2}{9}(\epsilon_0 - \epsilon_1)^2 f \left[\frac{2\pi a}{\lambda} \right]^3 \ll (\epsilon_0 - \epsilon_1)^2 f \ . \tag{2.6}$$

Because both values $(\epsilon_0 - \epsilon_1)^2$ and f are usually less than unity, the parameter α is a small value of the order of 10^{-2}–10^{-3} for such media as suspensions of solid spheres in liquids or pressed powders.[5,8,9] Below we shall use the smallness of this parameter in the calculations.

As far as linear optical properties are concerned, all the above expressions are also valid for a polycrystal sample, e.g., for a pressed powder prepared from a transparent single crystal with a nonzero second-order nonlinear polarizability $\chi^{(2)}$.[13] In this case small air cavities between single-crystal particles of a powder play the role of scatterers. However, the nonlinear properties of such a sample differ strongly from those of a single crystal. The reason is that the nonlinear polarizability $\langle \chi^{(2)}_{i,jl} \rangle$ averaged over all possible orientations of single-crystal particles turns out to be zero. Indeed, after such averaging the third-rank tensor $\langle \chi^{(2)}_{i,jl} \rangle$ becomes invariant under transformations of the group of rotations SO(3) in the three-dimensional space. The only nontrivial SO(3)-invariant third-rank tensor is known to be the totally antisymmetric tensor e_{ijl}. On the other hand, the tensor $\chi^{(2)}_{i,jl}(\omega,\omega)$ is symmetric with respect to indices, j,l. That is why for a polycrystal nonlinear sample one has $\langle \chi^{(2)}_{i,jl} \rangle = 0$. It means that for such samples a model with a constant in space nonlinear polarizability is principally wrong.

The more realistic model appropriate to this case is the one with a Gaussian random nonlinear polarizability $\chi^{(2)}(\mathbf{r})$, which is characterized by a correlator,

$$K(|\mathbf{r}-\mathbf{r}'|) = \langle \chi^{(2)}(\mathbf{r}) \chi^{(2)}(\mathbf{r}') \rangle = \langle \chi^2 \rangle \exp\left[-\frac{|\mathbf{r}-\mathbf{r}'|}{R} \right], \tag{2.7}$$

where R is an average size of single-crystal particle in a polycrystal and $\langle \chi^2 \rangle$ is a square of the nonlinear polarizability $\chi^{(2)}$ of the corresponding single crystal averaged over all possible orientations. For the sake of simplicity we omit the tensor structure of $\langle \chi^2 \rangle$ and consider it to be a scalar value.

III. THE EXPERIMENTAL GEOMETRY

We consider SHG in a slab of the thickness $L \gg l_\omega, l_{2\omega}$ (Fig. 1) occupying the layer $0 < z < L$. A plane monochromatic wave of the fundamental frequency ω is incident from the half space $z < 0$, the direction of incidence being in the x-z plane. We are interested in the angular distribution of the SH-light flux $\Pi_{2\omega}(\theta)$ radiated back into the half space $z < 0$. It is convenient to introduce a dimensionless quantity (nonlinear albedo)

$$R_{2\omega}(\theta) = \frac{\Pi_{2\omega}(\theta)}{\Pi_\omega} \ , \tag{3.1}$$

where Π_ω is a flux of an incident fundamental light. Because for linear diffuse scattering the value of the albedo is of the order of $1/2\pi$,[9] the quantity $2\pi R_{2\omega}$ gives a ratio of the generated SH flux to the flux of a scattered fundamental light.

The basic wave equations for the electric-field amplitudes of a fundamental and a SH light have the form

$$\nabla^2 \mathbf{E}_{2\omega} + \frac{4\omega^2}{c^2} \epsilon_{2\omega}(\mathbf{r}) \mathbf{E}_{2\omega} + \nabla \left[\frac{\nabla \epsilon_{2\omega}}{\epsilon_{2\omega}} \mathbf{E}_{2\omega} \right] = -\eta_{i,jl}(\mathbf{r}) E^{(j)}_\omega(\mathbf{r}) E^{(l)}_\omega(\mathbf{r}) \ , \tag{3.2}$$

$$\nabla^2 \mathbf{E}_\omega + \frac{\omega^2}{c^2} \epsilon_\omega(\mathbf{r}) \mathbf{E}_\omega + \nabla \left[\frac{\nabla \epsilon_\omega}{\epsilon_\omega} \mathbf{E}_\omega \right] = \mathbf{J}_\omega(\mathbf{r}) \ , \tag{3.3}$$

where

$$\eta_{i,jl} = \chi^{(2)}_{i,jl} \left[\frac{16\pi\omega^2}{c^2} \right] , \tag{3.4}$$

and $\mathbf{J}_\omega(\mathbf{r})$ is an external source of a fundamental light.

The vector nature of an electromagnetic field makes Eqs. (3.2) and (3.3) rather complicated. In particular, a

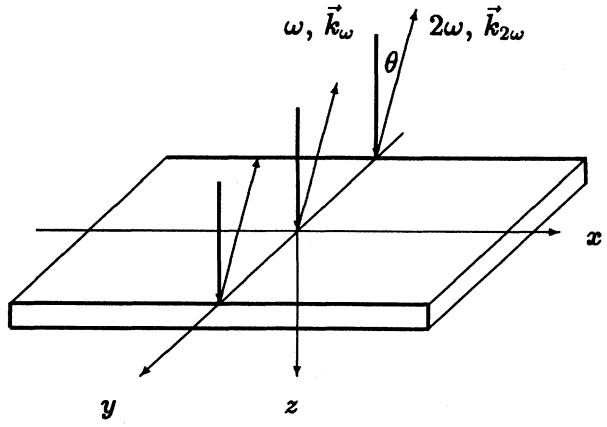

FIG. 1. The experimental geometry.

special term appears containing the logarithmic derivative of $\epsilon(\mathbf{r})$, which is due to the lack of transversality of an electric field in an inhomogeneous medium.[16] This term is responsible for the change in the polarization of light propagating in a disordered medium. Though polarization effects are important, they are known to be minimized (for linear backscattering) when the polarizations of an incident and a measured scattered light are the same, the electric field being parallel to the boundary of a sample (s polarizations).[9] For the same reason, the polarization effects in SHG are expected to be less important for the case where both a fundamental and a measured SH light is s polarized [$\mathbf{E}=(0,E,0)$] and, in addition, the nonlinear polarizability $\chi^{(2)}_{i,jl}$ satisfies the condition

$$\chi^{(2)}_{i,yy}=\chi^{(2)}\delta_{iy} \ . \tag{3.5}$$

This condition means that the nonlinear source on the right-hand side of Eq. (2.2) is polarized mainly in the y direction as is the linear source in (2.3).

The condition (2.4) is obviously fulfilled when a sample has a symmetry axis that coincides with the y axis. Practically, such a situation takes place when a static electric field is applied along the y axis to a powder of centrosymmetric crystal pressed into the form of a slab. For such a geometry one can use a simplified scalar model described by the equations

$$\nabla^2 E_{2\omega}+\frac{4\omega^2}{c^2}\epsilon_{2\omega}(\mathbf{r})E_{2\omega}=-\eta(\mathbf{r})E^2_{\omega}(\mathbf{r}) \ , \tag{3.6}$$

$$\nabla^2 E_{\omega}+\frac{\omega^2}{c^2}\epsilon_{\omega}(\mathbf{r})E_{\omega}=J_{\omega}(\mathbf{r}) \ . \tag{3.7}$$

This is just the model we will study below.

IV. THE DIAGRAMMATIC TECHNIQUE

The formal solution of Eqs. (3.6) and (3.7) may be expressed in terms of the corresponding Green functions $\mathcal{G}_{\omega}(\mathbf{r},\mathbf{r}')$ and $\mathcal{G}_{2\omega}(\mathbf{r},\mathbf{r}')$, each $\mathcal{G}(\mathbf{r})$ being dependent on the particular choice of random functions $\epsilon_{\omega}(\mathbf{r})$ and $\epsilon_{2\omega}(\mathbf{r})$, respectively:

$$E_{2\omega}=-\eta\{\hat{\mathcal{G}}_{2\omega}\{\hat{\mathcal{G}}_{\omega}J_{\omega}\}^2\} \ , \tag{4.1}$$

where $\{\hat{\mathcal{G}}J\}$ means a convolution. This operator equation corresponds to the diagram shown in Fig. 2(a). Here solid lines denote Green functions $\mathcal{G}_{\omega\,(2\omega)}(\mathbf{r},\mathbf{r}')$. Black circles correspond to fundamental-light sources J_{ω}, and an open circle corresponds to the nonlinear constant η. The SH intensity averaged over the ensemble of random functions $\epsilon(\mathbf{r})$ is given by the value $\langle|E_{2\omega}|^2\rangle$. Therefore, for a model with a nonrandom nonlinear constant η, one should average a product of six Green functions in order to obtain the SH intensity. This averaging may be represented by the diagrams shown in Figs. 2(b)–2(f), which are similar to those used in the theory of disordered conductors.[17,18] Here thin solid lines correspond to the averaged Green functions $G_{\omega\,(2\omega)}(z,z';\boldsymbol{\rho}-\boldsymbol{\rho}')$. At small values of the parameter α, the Fourier transforms,

$$G_{\omega,(2\omega)}(z,z';\mathbf{q})=\int G_{\omega,(2\omega)}(z,z';\boldsymbol{\rho}-\boldsymbol{\rho}')e^{i\mathbf{q}(\rho-\rho')}\frac{d\mathbf{q}}{(2\pi)^2} \ , \tag{4.2}$$

are given by

$$G_{\omega(2\omega)}(z,z';\mathbf{q}) =\frac{1}{2i\tilde{k}_{1,(2)}(q)}[e^{i|z-z'|\tilde{k}_{1,(2)}(q)}+r_{1,(2)}(q)e^{i(z+z')\tilde{k}_{1,(2)}(q)}] \ , \tag{4.3}$$

where

$$\tilde{k}(q)=\sqrt{\tilde{k}^2-q^2} \tag{4.4}$$

and

$$\tilde{k}_{1,(2)}=k_{1,(2)}+\frac{i}{2l_{\omega,(2\omega)}} \ . \tag{4.5}$$

In (4.3) and (4.5) k_1 and k_2 are wave vectors of a fundamental and a SH light in an effective transparent medium,

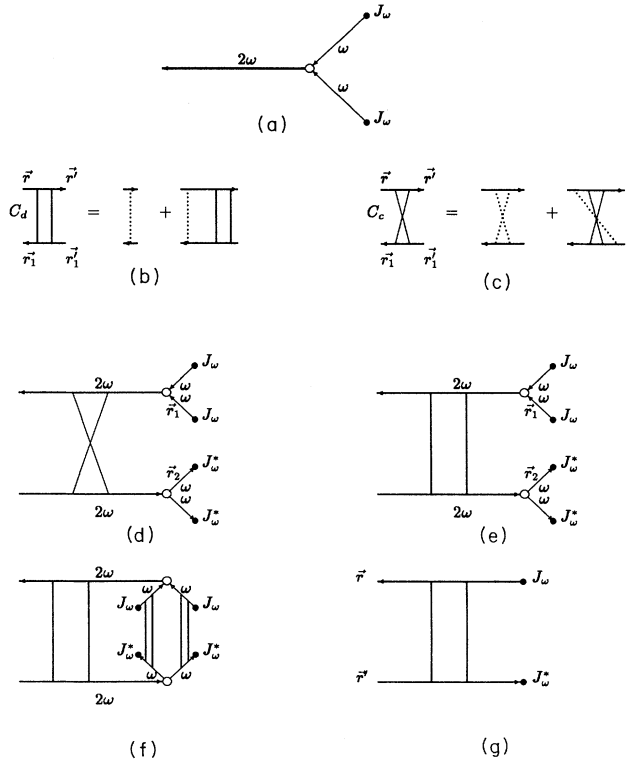

FIG. 2. The diagrammatic technique: (a) a diagrammatic representation for the SH-amplitude, (b) ladder and (c) maximally crossed diagrams, (d) a peak contribution to the SH intensity, (e) a surface and (f) a bulk contribution to the diffuse background, and (g) a diagrammatic representation for the field correlator $I_{\omega}(\mathbf{r},\mathbf{r}')$.

$$k_1=\frac{\omega}{c}\sqrt{\bar{\epsilon}_\omega},\quad k_2=\frac{2\omega}{c}\sqrt{\bar{\epsilon}_{2\omega}}\ . \tag{4.6}$$

The first term in (4.3) describes the bulk part of Green functions, while the second one is due to the internal reflection of light from the sample boundary, $r(q)$ being the complex reflectivity. The imaginary parts of $\tilde{k}_1$ and $\tilde{k}_2$ in (4.5) are due to light scattering, which results in an exponential decay of bulk parts of Green functions for $|z-z'|\gg l$ as well as a decay of surface-induced parts far away from the boundary $z,z'\gg l$.

However, averaging over a disorder does not reduce to independent averaging of Green functions. In addition, some correlations between different Green functions $\mathcal{G}(\mathbf{r},\mathbf{r}')$ should be taken into account. They are shown by dotted lines in Fig. 2, each dotted line corresponding to a correlator $\langle\delta\epsilon(\mathbf{r})\delta\epsilon(\mathbf{r}')\rangle$. At a multiple scattering diffusion regime, a special role is played by the infinite series $C_{d,(c)}(\mathbf{r},\mathbf{r}';\mathbf{r}_1,\mathbf{r}_1')$ of ladder and maximally crossed diagrams shown in Figs. 2(b) and 2(c). In the presence of time-reversal symmetry, both series can be expressed[9] in terms of a diffusion propagator $\mathcal{D}(\mathbf{r},\mathbf{r}')$:

$$C_d(\mathbf{r},\mathbf{r}';\mathbf{r}_1\mathbf{r}_1')=C_c(\mathbf{r},\mathbf{r}';\mathbf{r}_1',\mathbf{r}_1)=\frac{12\pi}{l^3}\mathcal{D}(\mathbf{r},\mathbf{r}')\delta(\mathbf{r}-\mathbf{r}_1)\delta(\mathbf{r}'-\mathbf{r}_1')\ . \tag{4.7}$$

An exact diffusion propagator is a solution of an integral equation corresponding to the ladder series [Fig. 2(b)]. The kernel of this equation depends on the surface-induced parts of Green functions (4.3), and a general equation is too complicated to be solved analytically. The only case where an analytical solution is possible corresponds to a negligible internal reflectivity $r(q)$. In this case the integral equation is of the Wiener-Hopf type. However, even a solution of this simplified equation is still too complicated for further analytical calculations. Therefore, in this paper we restrict ourselves to a simple approximate solution for the diffusion propagator $\mathcal{D}(\mathbf{r},\mathbf{r}')$. In accordance with this approximation[8-11] the diffusion propagator is supposed to satisfy a usual equation for the stationary case:

$$\nabla^2\mathcal{D}(\mathbf{r},\mathbf{r}')=-\delta(\mathbf{r}-\mathbf{r}')\ . \tag{4.8}$$

The effect of a boundary is taken into account by means of the following boundary conditions:

$$\mathcal{D}(\mathbf{r},\mathbf{r}')+h\frac{\partial\mathcal{D}(\mathbf{r},\mathbf{r}')}{\partial n}=0\ . \tag{4.9}$$

The constant h in Eq. (4.9) depends on the reflectivity of a boundary and on the corresponding elastic-scattering length l. For small values of the reflectivity, a comparison of the approximate solution with the exact one far away from the boundary gives the following value of the constant h:[9,12]

$$h_{1,(2)}\approx 0.7l_{\omega,(2\omega)}\ . \tag{4.10}$$

For the case $L\gg l,z,z'$, the Fourier-transform $\mathcal{D}(z,z';q)$, which we shall use in our further calculations, is given by

$$\mathcal{D}(z;z';q)=\frac{1}{2q}\left[e^{-q|z-z'|}-\frac{1-qh}{1+qh}e^{-q(z+z')}\right]\ . \tag{4.11}$$

In Fig. 2 only diagrams with the minimal number of diffusion propagators are shown. More complicated diagrams containing a larger number of diffusion propagators are proportional to additional small factors $\alpha\ll 1$ [see (2.6)]. In calculating diagrams one also should take into account that each external Green function originating at a source corresponds to the factor $\{\hat{G}_\omega,J_\omega\}=\langle E_\omega\rangle$, where $\langle E_\omega\rangle$ is an averaged electric field inside the sample. For nearly normal incidence it is given by

$$\langle E_\omega\rangle=E_\omega^{(0)}\exp\left[i\mathbf{k}\cdot\mathbf{r}-\frac{z}{2l_\omega}\right]\ , \tag{4.12}$$

where $\mathbf{k}_1$ is a wave vector of an incident fundamental light. For the correct calculation of the nonlinear albedo (3.1) near the backscattering direction ($\theta\ll 1$), one should prescribe the function

$$\frac{1}{4\pi E_\omega^{(0)}}\sqrt{T_{2\omega}/S}\exp\left[-i\mathbf{k}_2\cdot\mathbf{r}-\frac{z}{2l_{2\omega}}\right] \tag{4.13}$$

to external lines corresponding to SH Green functions. In this equation, $T_{2\omega}$ is a transmission coefficient for the SH-light incident on a sample from the outside, S is an illuminated area of a sample, and $\mathbf{k}_2$ is a wave vector of an outgoing SH light.

It can be easily seen that Figs. 2(d) and 2(e) correspond to processes when a fundamental light is not scattered before nonlinear mixing. Due to the exponential decay of the averaged electric field (4.12), the main contribution of these diagrams corresponds to the surface SHG, which occurs within a layer of thickness l_ω near the boundary of a sample. On the contrary, in Fig. 2(f), the nonlinear-mixing point is separated from external-source points by an infinite number of scattering events. This diagram describes the bulk SHG by nonlinear mixing of the multiple-scattered fundamental-light photons. Using (4.7) and (4.13), one can see that only Fig. 2(d) depends on the direction of the SH wave vector $\mathbf{k}_2$. It is this diagram that describes the interference peak in the SH intensity in the direction corresponding to $\mathbf{k}_2=-2\mathbf{k}_1$.[10] All other diagrams of Fig. 2 contribute to the diffuse background in the angular distribution of the SH intensity.

V. THE CALCULATION OF DIAGRAMS

We calculate the diagrams of Fig. 2 for the case when a fundamental light is incident normally on the boundary $z=0$ of a sample. In this case only Fourier components $G(z,z';q=0)=G(z,z')$ contribute to the result and the calculations are simplified considerably. In particular, the diagrams shown in Figs. 2(e) and 2(d) correspond to the following expressions, which one can obtain using (4.7), (4.12), and (4.13):

$$R_0 = A\int_0^L dz dz' dz_1 dz_2 e^{-(z_1+z_2)/l_\omega} e^{-z/l_{2\omega}} e^{2ik_1(z_1-z_2)} \mathcal{D}_{2\omega}(z,z';q=0) G_{2\omega}(z',z_1) G^*_{2\omega}(z',z_2) , \tag{5.1}$$

$$R_p(\theta) = A\int_0^L dz dz' dz_1 dz_2 e^{-(z_1+z_2)/l_\omega} e^{-(z+z')/2l_{2\omega}} e^{2ik_1(z_1-z_2)} e^{-ik_2(z-z')} \mathcal{D}_{2\omega}(z,z';q) G_{2\omega}(z,z_1) G^*_{2\omega}(z',z_2) , \tag{5.2}$$

where $q=(k_2)_x$ is a small component of the SH wave vector $\mathbf{k}_2$ parallel to the boundary,

$$q \approx \frac{2\omega}{c}|\theta| , \tag{5.3}$$

and the coefficient A is given by

$$A = \frac{12\pi}{l_{2\omega}^3} T_{2\omega} (\chi^{(2)} |E_\omega^{(0)}|)^2 \left[\frac{2\omega}{c}\right]^4 . \tag{5.4}$$

Because the diffusion propagator (4.11) decreases with increasing q, the function $R_p(\theta)$ has a peak at $\theta=0$ (see Figs. 1, 7, and 8). This is just an interference peak in the SH intensity, which we predict to occur.

For the case of interest, $L \gg l_{2\omega}$, the upper limit of integration in (5.1) and (5.2) can be chosen to be infinity. The independence of the integrals on the thickness of a sample for $L \gg l_{2\omega}$ means that the diagrams of Figs. 2(d) and 2(e) describe a surface contribution to the SH intensity. At a small value of the parameter $\alpha_{2\omega}$ the quantities $R_p(\theta)$ and R_0 do not depend explicitly on the reflectivity of a boundary r (but do depend on h). The results of the calculations may be expressed in terms of the following dimensionless parameters:

$$\zeta = h_2 / l_{2\omega} , \tag{5.5}$$

$$\mu = \frac{1}{2} + \frac{l_{2\omega}}{l_\omega} , \tag{5.6}$$

and

$$\Delta = (k_2 - 2k_1) l_{2\omega} . \tag{5.7}$$

The possible values of parameters μ and ζ may be found from (2.5) and (4.10). For the case of Rayleigh scattering ($a \ll \lambda$) with no significant internal reflection of SH light from the interface, parameters ζ and μ are equal to

$$\zeta_{\min} \approx 0.7, \quad \mu_{\min} = \tfrac{9}{16} . \tag{5.8}$$

With increasing the internal reflection the parameter ζ also increases, ζ being proportional to $T_{2\omega}^{-1}$ at small $T_{2\omega}$. The increase in sizes of scatterers gives rise to an increase in the parameter μ. When the sizes approach the wavelength, the ratio $l_{2\omega}/l_\omega$ tends to unity, so that the parameter μ takes a maximum value

$$\mu_{\max} = \tfrac{3}{2} . \tag{5.9}$$

The final result of calculating (5.2) reads

$$R_p(\theta) = \frac{3\pi}{2} T_{2\omega} (\chi^{(2)} |E_\omega^{(0)}|)^2 \left[\frac{2\omega}{c}\right]^4 \left[\frac{l_{2\omega}}{k_2}\right]^4 \left[\frac{l_{2\omega}}{k_2}\right]^2 \frac{f(\bar{q})}{[(\mu+\bar{q})^2+\Delta^2](1+\bar{q})^2} , \tag{5.10}$$

where

$$f(\bar{q}) = \frac{2\zeta}{1+\bar{q}\zeta} + \frac{\Delta^2+(\mu+\bar{q})^2+\mu^{-1}(1+2\mu+\bar{q})^2}{\Delta^2+(1+\mu)^2} \tag{5.11}$$

and

$$\bar{q} = q l_{2\omega} = \frac{2\omega l_{2\omega}}{c}|\theta| = |\theta|/\alpha_{2\omega} . \tag{5.12}$$

Expressions (5.10)–(5.12) show that the angular width of the interference peak is of the order of $\Delta\theta = \alpha_{2\omega}$ and the peak shape depends on parameters μ, ζ and Δ (see Figs. 7 and 8). On the contrary, expression (5.1) does not depend on the angle θ. It describes a part of a diffuse background in the angular distribution of SH intensity.

The crucial parameter for the observation of the predicted peak is a peak-to-background ratio, which depends on parameters of a system and may be considerably less than two. In order to evaluate this quantity one should calculate the integral (5.1) and compare it with the $q=0$ limit of the expression (5.10). The result may be represented in the form

$$R_0 = \frac{3\pi}{2} T_{2\omega} (\chi^{(2)} |E_\omega^{(0)}|)^2 \left[\frac{2\omega}{c}\right]^4 \left[\frac{l_\omega l_{2\omega}}{k_2^2}\right] \frac{f_0(\mu,\zeta)(\mu_0^2+\Delta^2)}{(\mu^2+\Delta^2)[(\mu+1)^2+\Delta^2]} , \tag{5.13}$$

$$R_p(0) = \frac{3\pi}{2} T_{2\omega} (\chi^{(2)} |E_\omega^{(0)}|)^2 \left[\frac{2\omega}{c}\right]^4 \left[\frac{l_{2\omega}}{k_2}\right]^2 \frac{(1+2\zeta)(\mu_p^2+\Delta^2)}{(\mu^2+\Delta^2)[(\mu+1)^2+\Delta^2]} , \tag{5.14}$$

where

$$f_0(\mu,\zeta) = \frac{(2+4\zeta)\mu^2-\mu+1}{2\mu} , \tag{5.15}$$

$$\mu_0^2 = \frac{\mu^2(\mu+1)[(2+4\zeta)\mu+5+4\zeta]}{(2+4\zeta)\mu^2-\mu+1} , \tag{5.16}$$

$$\mu_p^2 \frac{(\mu+1)[(1+2\zeta)\mu^2+(3+2\zeta)\mu+1]}{(1+2\zeta)\mu} . \tag{5.17}$$

The bulk contribution $R_0^{(\text{bulk})}$ to the diffuse background given by Fig. 2(f), can be expressed in terms of the field correlator:

$$I_\omega(\mathbf{r},\mathbf{r}')=\frac{\langle E_\omega(\mathbf{r})E_\omega^*(\mathbf{r}')\rangle}{|E_\omega^{(0)}|^2} . \tag{5.18}$$

Comparing the diagrams of Figs. 2(f) and 2(g), one obtains

$$R_0^{(\text{bulk})}=\frac{T_{2\omega}}{S}(\chi^{(2)}|E_\omega^{(0)}|)^2\left[\frac{2\omega}{c}\right]^4\int d^3\mathbf{r}\int d^3\mathbf{r}'[I_\omega(\mathbf{r},\mathbf{r}')]^2 I_{2\omega}(\mathbf{r},\mathbf{r}') . \tag{5.19}$$

In the bulk region the field correlator (5.18) is given by the expression[10]

$$I_{\omega(2\omega)}(\mathbf{r},\mathbf{r}')=I_0(z)\frac{\sin[k_{1(2)}|\mathbf{r}-\mathbf{r}'|]}{k_{1(2)}|\mathbf{r}-\mathbf{r}'|}\exp\left[\frac{k_{1(2)}|\mathbf{r}-\mathbf{r}'|}{2l_{\omega(2\omega)}}\right] , \tag{5.20}$$

where $I_0(z)$ is an averaged intensity of light in a sample

$$I_0(z)=3(1+\zeta)(1-z/L) . \tag{5.21}$$

Using Eqs. (5.20) and (5.21), the integral in (5.19) may be represented as follows:

$$\frac{27\pi}{2}(1+\zeta)^3\frac{SL}{k_1^2k_2}[2I(k_2)-I(2k_1+k_2)-I(k_2-2k_1)] , \tag{5.22}$$

where

$$I(k)=\int_0^\infty \frac{\sin\left[\frac{kl_{2\omega}}{\mu}t\right]}{t}e^{-t}dt=\tan^{-1}\left[\frac{kl_{2\omega}}{\mu}\right] . \tag{5.23}$$

At small values of $\alpha_{2\omega}$ one can set $I(k_2)=I(2k_1+k_2)=\pi/2$. Then Eqs. (5.19)–(5.23) result in

$$R_0^{(\text{bulk})}=\frac{27\pi}{2}(1+\zeta)^3T_{2\omega}(\chi^{(2)}|E_\omega^{(0)}|)^2\frac{L}{k_1^2k_2}\left[\frac{2\omega}{c}\right]^4\cot^{-1}\left[\frac{\Delta}{\mu}\right] . \tag{5.24}$$

It is seen from Eq. (5.24) that the contribution $R_0^{(\text{bulk})}$ becomes the main one at large values of L. In this limit the interference-peak intensity is small as compared to that of diffusive background. However, for intermediate values of sample thickness $l_{2\omega}\ll L<L_0(\Delta)$, where

$$L_0(0)\sim 2\pi l_{2\omega}l_\omega/\lambda=\frac{l_{2\omega}}{\alpha_\omega}\gg l_{2\omega} , \tag{5.25}$$

one can neglect the process of SHG by a scattered fundamental light. For such samples the peak-to-background ratio takes the form

$$\frac{R_{2\omega}(0)-R_0}{R_0}=\frac{(1+2\zeta)(\mu_p^2+\Delta^2)}{f_0(\mu,\zeta)(\mu_0^2+\Delta^2)}\left[\frac{l_{2\omega}}{l_\omega}\right] . \tag{5.26}$$

It follows from (5.26) that the peak-to-background ratio decreases with increasing l_ω. Therefore, one can conclude that scattering of a fundamental light results in an increase in the relative value of the interference peak.

VI. THE EFFECT OF A PHASE-MATCHING CONDITION

In this section we consider the influence of the frequency dispersion of $\bar{\epsilon}(\omega)$ on the results obtained. It is well known that one of the main difficulties of the SHG experiments is connected with a nonzero value of $2k_1-k_2=(2\omega/c)(\sqrt{\bar{\epsilon}_{2\omega}}-\sqrt{\bar{\epsilon}_\omega})$. For the case of SHG in a transparent medium, the phase-matching condition should be fulfilled with the accuracy of

$$|2k_1-k_2|<L^{-1} , \tag{6.1}$$

otherwise the SHG intensity is negligible. However, the requirement (6.1) becomes weaker in strongly scattering media, as it follows from (5.13), (5.14), and (5.24). A considerable decrease in the intensities R_0 and $R_p(0)$ occurs when

$$|2k_1-k_2|>l_{2\omega}^{-1} . \tag{6.2}$$

The reason is that the uncertainty of wave vectors in a strongly scattering medium is of the order of the inverse scattering length, rather than the inverse size of a sample.

An interesting phenomenon takes place in a relatively thick sample with $L>L_0(\Delta)$. Equation (5.24) shows that the intensity of the diffuse background behaves like $\cot^{-1}(k_2-2k_1)l_{2\omega}$. Therefore, there is no decrease in the SHG intensity at large positive $(2k_1-k_2)l_{2\omega}$, while at large negative $(2k_1-k_2)l_{2\omega}$ the intensity decreases proportional to $|2k_1-k_2|^{-1}$. The explanation of such an

asymmetry is rather simple. In the bulk of a sample there are fundamental-light photons with all possible directions of momenta. The total momentum should be conserved [see Fig. 4(d)] in a process of SHG with the accuracy of $l_{2\omega}^{-1}$. This means that a considerably SHG can occur only when the following condition is fulfilled:

$$|\mathbf{k}_1+\mathbf{k}_1'|\approx k_2, \quad |\mathbf{k}_1|=|\mathbf{k}_1'|=k_1 , \tag{6.3}$$

where $\mathbf{k}_1$ and $\mathbf{k}_1'$ are wave vectors of two mixing fundamental photons. For the case when $2k_1>k_2$, the condition (6.3) can always be fulfilled by a proper choice of the angle between wave vectors $\mathbf{k}_1$ and $\mathbf{k}_1'$, while for $2k_1<k_2$ it is impossible to meet this requirement.

A relatively slow (if any) decrease in $R_0^{(\text{bulk})}$ with increasing $|\Delta|$ means that at sufficiently large values of $|\Delta|>1$ this contribution to $R_{2\omega}(\theta)$ always becomes the main one. For $|\Delta|\gg L_0(0)/L$ the interference peak can hardly be observed because of its small relative value. However, as long as the sample thickness L is still less than $L_0(\Delta)$, the dependence of the peak-to-background ratio on $|\Delta|$ is not too strong (see Fig. 6).

On the other hand, the effect of an absence of SHG suppression at $\Delta<0$ in strongly scattering media can be used to increase the integral SHG intensity. Indeed, using the expressions (4.12) and (4.13) and calculating Fig. 2(a), one can show that for a Gaussian profile of the incident beam intensity in the x-y plane, the integral SH intensity $I=\int R_{2\omega}(\theta)d\Omega$ generated in a transparent sample is equal to

$$I_{\text{tr}}=(4\pi)^2(\chi^2|E_\omega^{(0)}|)^2L\left[\frac{\omega}{c}\right]\frac{\sin[(\omega/c)(\Delta n)L]}{(\Delta n)} . \tag{6.4}$$

Using the expression (5.24) also, we obtain the ratio of the integral SH intensities I_{sc} and I_{tr} generated in a strongly scattering and in a transparent sample. At large negative values of $\Delta=(2\omega l_{2\omega}/c)(\Delta n)$ it has the form

$$I_{\text{sc}}/I_{\text{tr}}=\frac{27\pi}{2}(1+\zeta)^3|\Delta n|\approx 200|\Delta n| . \tag{6.5}$$

It is seen that for $|\Delta n|>5\times10^{-3}$ the total SH intensity generated in a strongly scattering sample is larger than that generated in a transparent sample.

VII. THE MODEL WITH A RANDOM NONLINEAR POLARIZABILITY

The model with a constant in space nonlinear polarizability, which has been considered above, fails to explain SHG in a polycrystal sample. In this section we study the model with a random nonlinear polarizability $\chi^{(2)}(\mathbf{r})$, which is characterized by the correlator (2.7). We shall concentrate on the calculation of the surface contributions to $R_{2\omega}$ similar to those described by the diagrams shown in Figs. 2(d) and 2(e). However, in the case of a random nonlinear polarizability, the integrations over positions of nonlinear-mixing points $\mathbf{r}_1$ and $\mathbf{r}_2$ are no longer independent due to the correlator $K(|\mathbf{r}_1-\mathbf{r}_2|)$. The diagrams corresponding to those of Figs. 2(e) and 2(d) are shown in Fig. 3(a) and Fig. 3(b), respectively. It is worth noting that in a general case where there is both a nonzero average value and a random part of the nonlinear polarizability, the same diagrams appear *in addition* to the diagrams of Fig. 2. Below we consider a case when the correlation radius R obeys the following condition:

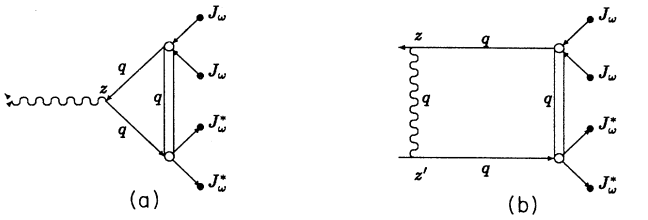

FIG. 3. The diagrammatic representation of SH-intensity for the case of a random nonlinear polarizability: (a) a diagram for the interference peak and (b) a surface contribution to the diffuse background; double lines denote the correlator of nonlinear polarizabilities, and wavy curves correspond to diffusion propagators.

$$\lambda<R\ll l_{2\omega} . \tag{7.1}$$

This condition is most likely fulfilled in experiments on powder samples[13] where R is an average size of powder particles. It is seen from Fig. 3 that under such a condition the main contribution of the diagram Fig. 3(b) corresponds to the integration over large momenta $q\sim R^{-1}\gg l^{-1}$. In this case the diffusion approximation (4.8) and (4.9) no longer holds for the diffusion propagator $\mathcal{D}(z,z';q)$, which is determined mainly by twofold scattering. At $zq\gg1$ and $z'q\gg1$ one can neglect the surface-induced term in the diffusion propagator and use the bulk expression for $\mathcal{D}(z,z';q)$, which decreases strongly when $|z-z'|>q^{-1}$. Because in the further calculations the diffusion propagator is to be integrated over an interval $|z-z'|\gg q^{-1}$, the following approximation for $\mathcal{D}(z,z';q)$ is sufficient for the calculation of Fig. 3(b)

$$\mathcal{D}(z,z';q\gg l^{-1})=\delta(z-z')\frac{\pi}{6}\frac{l_{2\omega}}{q} . \tag{7.2}$$

On the contrary, in Fig. 3(a), the longitudinal momentum q in the diffusion propagator remains equal zero. Therefore, the diffusion propagator for this diagram is given by the $q=0$ limit of the expression (4.11):

$$\mathcal{D}(z,z';q=0)=\frac{(z+z')-|z-z'|}{2}+h . \tag{7.3}$$

The contributions R_0 and $R_p(\theta)$ of both diagrams of Fig. 3 can be expressed in terms of the quantity

$$F(z,z';q)=\int_0^\infty dz_1dz_2K(z_1,z_2;q)G_{2\omega}(z,z_1;q)G_{2\omega}^*(z',z_2;q)e^{2ik_1(z_1-z_2)-(z_1+z_2)/l_\omega} , \tag{7.4}$$

where $K(z_1,z_2;q)$ is a longitudinal Fourier-component of the correlator (2.7):

$$R_0 = A\int_0^\infty dzdz''\int \frac{dq}{(2\pi)^2}\mathcal{D}(z'',z;q=0)F(z,z;q)e^{-z''/l_{2\omega}}, \tag{7.5}$$

$$R_p(0) = A\int_0^\infty dzdz'\int \frac{dq}{(2\pi)^2}\mathcal{D}(z,z';q)F(z,z';q)e^{-ik_2(z-z')}e^{-(z+z')/2l_{2\omega}}. \tag{7.6}$$

Neglecting all terms proportional to the higher powers of small parameters λ/R or λ/l one can obtain the following expression for $F(z,z';q)$:

$$F(z,z';q) = \left[\frac{\pi R k_2^{-2} l^*}{q^2+|2k_1-k_2|^2+R^{-2}}\right] e^{ik_2(z-z')}e^{-(z+z')/l_\omega}(e^{-|z-z'|/l^*}-e^{-(z+z')/l^*}), \tag{7.7}$$

where

$$\frac{l}{l^*} = \frac{l}{2l_{2\omega}} - \frac{l}{l_\omega}. \tag{7.8}$$

It is seen from (7.7) that at $R \ll l$ the quantity $F(z,z';q)e^{-ik_2(z-z')}$ varies weakly at the variation of $z-z'$ by a value $q^{-1}\sim R$. That is why the approximation (7.2) with a δ function is valid. The rest part of calculations is trivial and the final result is:

$$R_0 = A\frac{Rl_\omega l_{2\omega}^3}{16\mu k_2^2}\ln\left[\frac{k_2^2}{|2k_1-k_2|^2+R^{-2}}\right](1+2\mu+4\mu\xi), \tag{7.9}$$

$$R_p(0) = A\frac{\pi^2}{48\mu}\frac{Rk_2^{-2}l_{2\omega}^3}{\sqrt{|2k_1-k_2|^2+R^{-2}}}, \tag{7.10}$$

where the constant A is given by Eq. (5.4). The expressions (7.9), (7.10), and (5.24) show that the peak-to-background ratio behaves like

$$\frac{R_{2\omega}(0)-R_0}{R_0} = \left[\frac{\pi^2\xi}{6l_\omega}\right]\frac{k_1Rl_\omega}{c_1k_1Rl_\omega + c_2L\cot^{-1}\left[\frac{\Delta}{\mu}\right]}, \tag{7.11}$$

where $c_1=(1+2\mu+4\mu\zeta)\ln(k_2\xi), c_2=18\mu(1+\zeta)^3$, and

$$\xi = \frac{R}{\sqrt{1+R^2|2k_1-k_2|^2}}. \tag{7.12}$$

The main result of these calculations is the following. Under the conditions (7.1), the peak-to-background ratio is considerably less than in the case of nonrandom nonlinear polarizability, and it decreases strongly with decreasing the correlation radius R or increasing the difference $|2k_1-k_2|$. It may be shown that simultaneously the angular width of the peak increases $\Delta\theta\sim\lambda/\xi \gg \lambda/l_{2\omega}$. It means that in powder samples the interference peak in SHG is smeared out. For example, in the experiment[13] the parameters of a sample satisfy the conditions $R\sim\xi\sim\lambda\approx 1$ μm and $\Delta\approx 50$. For such conditions the peak-to-background ratio is approximately equal to $0.02\Delta k_1R^2/L\sim 10^{-4}$, which is, of course, unobservable.

VIII. THE MAIN QUALITATIVE FEATURES OF SHG IN OPAQUE MEDIA

First of all we shall explain what is the cause of a peak in the angular distribution of SH intensity and why this peak is referred to as an "interference peak." Because of the supposed small ratio λ/l, the explanation can be done using the quasiclassical language of photon trajectories. In Fig. 4(a) the process of SHG is shown for the case when nonlinear-mixing points are situated in a layer of thickness $l_{2\omega}$ near the interface $z=0$. In this case for each trajectory of a SH photon one can always find a conjugated trajectory [depicted by a dotted line in Fig. 4(a)], both being connected by the time-reversal transformation. For such conjugated trajectories, a random difference in phases $\delta\varphi$ of the outgoing SH waves arises only due to the incomplete equivalence of their initial and final parts at a nonzero value of the difference $2k_1-k_2$. The corresponding phase-difference acquired on a distance $d\sim l_{2\omega}$ is of the order of $\delta\phi\sim\Delta$. If the parameter $|\Delta|$ is small, a constructive interference between the conjugated trajectories takes place, which doubles the contribution of these trajectories in a total SH intensity. It is clear that such an interference could occur only when the outgoing SH wave is directed oppositely to the incident fundamental one ($\theta=0$). Otherwise, an additional random difference in phases appears, which depends on the particular shape of the trajectory (more strictly, it depends on the distance between the points of the first and last scattering). After averaging over random positions of scatterers, all the interference terms containing a random difference in phases vanish. Therefore, contributions of all trajectories corresponding to sufficiently large angle θ are added incoherently. That is why there should be a peak in the angular distribution of SH intensity in the backward direction.

In fact, the nature of the interference peak is the same as for linear backscattering.[2-9] The only important

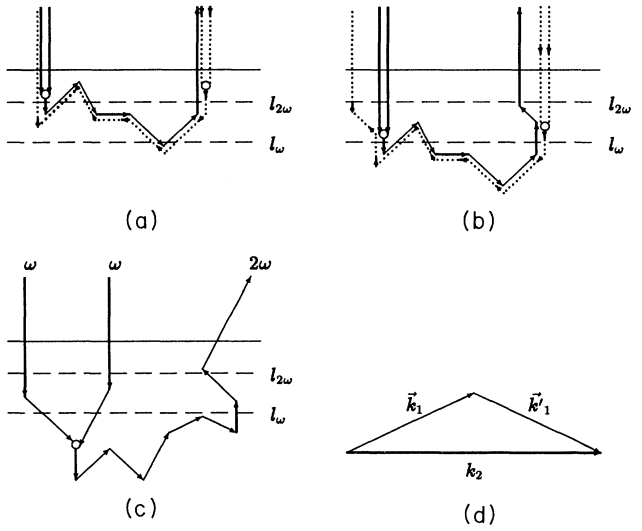

FIG. 4. Typical trajectories of photons for different processes of SHG: (a) conjugated trajectories contributing to the interference peak, (b) trajectories with no fundamental-light scattering contributing to the diffuse background, (c) a trajectory for SHG in the bulk, and (d) the momentum-conservation law.

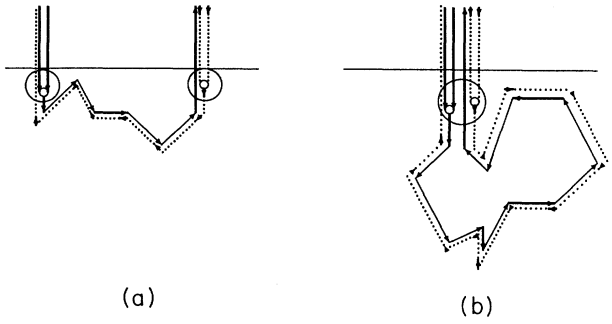

FIG. 5. Two different types of conjugated trajectories in a polycrystal sample: (a) nonlinear-mixing points are in different monocrystal particles (b) nonlinear-mixing points are in the same monocrystal particle.

difference is that a SH light is generated in a sample, not incident from the outside. This difference exhibits itself in the dependence of results on the phase-matching condition. It also manifests itself in the contribution of trajectories corresponding to nonlinear mixing in a layer $l_\omega > z > l_{2\omega}$ [see Fig. 4(b)]. Because SH photons have a small probability of ballistic motion through a layer of the thickness $l_\omega > l_{2\omega}$, for such trajectories there are no conjugated ones. Hence, these trajectories are added incoherently and they make no contribution to the interference peak. Nevertheless, all trajectories shown in Fig. 4(b) contribute to the diffuse background. Therefore, the peak-to-background ratio for the total SH-intensity is considerably less than two (which is typical for linear backscattering[2–9]) and depends on the ratio $l_\omega / l_{2\omega}$.

The next result to be explained is the suppression of SHG in the bulk, i.e., beyond a layer of the thickness l_ω [see Fig. 4(c)]. In this case two fundamental photons taking part in SHG are scattered, and, hence, they have arbitrary directions of their wave vectors $\mathbf{k}_1$ and $\mathbf{k}'_1$ just before nonlinear mixing. Therefore, the momentum-conservation law (6.3) cannot be fulfilled automatically in this case (even when $2k_1 = k_2$). It gives ruse to some constraint (within the uncertainty $\delta k \sim l_{2\omega}^{-1} \ll k$) in possible directions of the fundamental-photon wave vectors $\mathbf{k}_1$ and $\mathbf{k}'_1$ [see Fig. 4(d)]. It is this constraint that results in the suppression of SHG in the bulk by the appearance of an additional small factor λ / l in the expression for a SH intensity. That is why the peak-to-background ratio for not too thick samples is determined mainly by the ratio of thicknesses of a layer ($\sim l_{2\omega}$), where conjugated trajectories of SH photons are originated, and a layer ($\sim l_\omega$), which contributes mainly to the diffuse background.

Finally we give a qualitative explanation of a decrease in the peak-to-background ratio for polycrystal samples. In this case all conjugated trajectories of the Fig. 4(a) can be subdivided into two general classes. One of them consists of conjugated trajectories with nonlinear-mixing points being situated in different monocrystal particles [Fig. 5(a)]. Another class corresponds to conjugated trajectories with two nonlinear-mixing points being in the same monocrystal particle [Fig. 5(b)]. The interference term corresponding to conjugated trajectories of the Fig. 5(a) vanishes after averaging over random orientations of monocrystal particles due to the zero average value of the nonlinear polarizability. Therefore, such trajectories make no contribution to the interference peak. On the contrary, trajectories of Fig. 5(b) contribute to the peak intensity in the same way as in the case of a monocrystal sample. However, for small sizes of monocrystal particles $R \ll l_{2\omega}$, such trajectories correspond to random walks with a return to approximately the same point. In three-dimensional space (contrary to the case of two-dimensional space[1]) the probability of such processes is small by use of the parameter $R / l_{2\omega}$. Therefore, the peak-to-background ratio decreases by the same small factor in polycrystal samples.

IX. DISCUSSION

Because nonlinear effects are relatively small, one has to estimate an order of magnitude of the nonlinear albedo (3.1). As an appropriate model system, we consider an inhomogeneous centrosymmetric nonlinear material in an external electrostatic field E_0. A good example of such a material is the one containing semiconductor microcrystallites embedded in a glass matrix.[19,20] A value of $\chi^{(3)}$ of the order of 10^{-8} esu is typical for such materials. For the estimations made below, we take a value of the electrostatic field $E_0 \sim 300$ kV/cm $= 10^3$ esu and a value of the fundamental-light flux $\Pi_\omega \sim 10^4$ W/cm^2. At such intensities one has

$$\chi^{(2)} |E_\omega^{(0)}| = \chi^{(3)} E_0 |E_\omega^{(0)}| \sim 6 \times 10^{-5} . \quad (9.1)$$

Another important parameter $\alpha_{2\omega}^{-1}=2\omega l_{2\omega}/c$ is usually of the order of 10^2–10^3 in similar strongly scattering media.[2–9] For our estimations we choose $\lambda_{2\omega}=3{,}2\times10^{-5}$ cm and $l_{2\omega}=10^{-2}$ cm, so that $\alpha_{2\omega}^{-1}=2\times10^3$. Therefore, at $|2k_1-k_2|l_{2\omega}<1$ we obtain for the nonlinear albedo the following estimation:

$$R_{2\omega}\sim(\chi^{(2)}|E_{\omega}^{(0)}|\alpha_{2\omega}^{-1})^2\sim10^{-2}\ . \tag{9.2}$$

This means that the generated SH intensity can be as large as few percent of the scattered fundamental-light intensity. This is, of course, sufficient for the observation of second-harmonic generation.

The most serious experimental difficulty results from a small value of the peak-to-background ratio and large fluctuations of intensity due to a randomness of a medium. The latter fluctuations (speckles) may be so large in solid strongly scattering media that one fails to observe even a linear backscattering peak.[5] Nevertheless, averaging by means of rotation of a sample with respect to an incident beam, can reveal the predicted interference peak if the peak-to-background ratio is not too small.

In Fig. 6 the peak-to-background ratio is shown as a function of $\Delta=(k_2-2k_1)l_{2\omega}$ for different values of the parameter μ and different thicknesses of a sample. It is seen that the peak-to-background ratio is larger for thin samples ($L=1$ mm) corresponding to dashed ($\mu=\frac{9}{16}$) and dotted-dashed ($\mu=\frac{3}{2}$) lines, the relative value of the interference peak being especially large in the latter case of big scatterers ($a>\lambda$). However, in this case the peak-to-

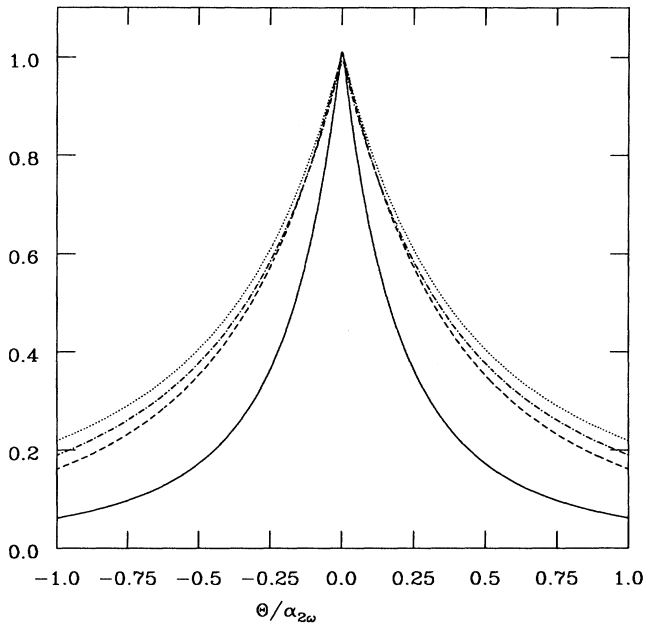

FIG. 7. The dependence of the normalized peak shape on Δ at $\mu=\frac{9}{16}$: the solid, dashed, and dotted lines correspond to $\Delta=0$, 1, and 10, respectively; the dotted-dashed line corresponds to the linear backscattering peak.

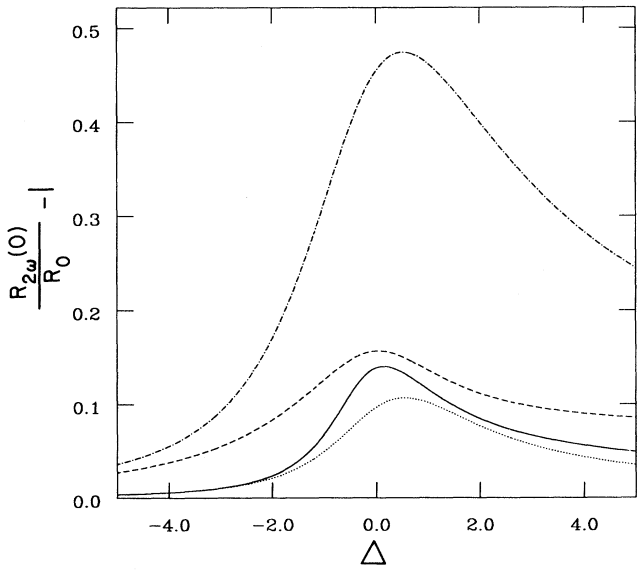

FIG. 6. The peak-to-background ratio as a function of Δ: the solid line corresponds to $L=1$ cm, $\mu=\frac{9}{16}$, the dashed line corresponds to $L=1$ mm, $\mu=\frac{9}{16}$, the dotted line corresponds to $L=1$ cm, $\mu=\frac{3}{2}$, and the dashed-dotted line corresponds to $L=1$ mm, $\mu=\frac{3}{2}$.

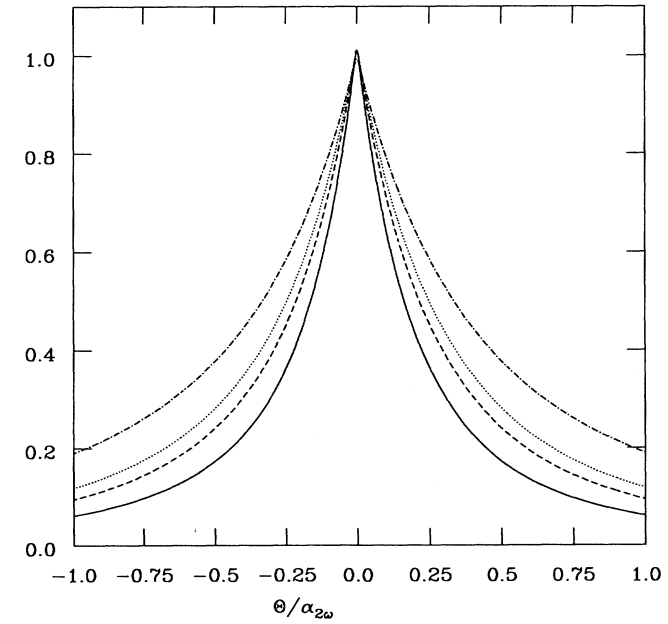

FIG. 8. The dependence of the normalized peak shape on μ at $\Delta=0$: the solid, dashed, and dotted lines correspond to $\mu=\frac{9}{16}$, 1, and $\frac{3}{2}$, respectively; the dotted-dashed line corresponds to the linear backscattering peak.

background ratio decreases rapidly when increasing the thickness of a sample (the dotted curve corresponds to $L=1$ cm), while for small scatterers ($\mu=\frac{9}{16}$) the dependence on a thickness is not so important (compare the dashed curve and the solid curve, which corresponds to $L=1$ mm and $L=1$ cm, respectively). It is also seen that the peak-to-background ratio is larger in the case of positive dispersion $\Delta>0$ when the bulk contribution to the diffuse background is suppressed more strongly.

The dependence of the peak shape on the parameters Δ and μ is shown in Fig. 7 and Fig. 8, respectively. At large values of $|\Delta|>1$, the peak shape is approximately the same as for linear backscattering of SH light, whereas for $|\Delta|\ll 1$ the peak width is considerably smaller.

The main results of this paper can be summarized as follows.

(1) The angular distribution of the SH intensity should exhibit a sharp peak in the backward direction as well as a diffuse background.

(2) For not too quick samples the peak-to-background ratio increases with increasing the size of scatters a until $a>\lambda$.

(3) For polycrystal samples with $\langle\chi^{(2)}\rangle=0$ and small sizes of monocrystal particles $R\ll l_{2\omega}$, the peak-to-background ratio is small.

(4) The SH intensity in a thick sample has a weak angular dependence, but it strongly depends on the sign of the frequency dispersion $\Delta n=n(2\omega)-n(\omega)$, where n is an average refraction index. For negative Δn the SH intensity does not decrease with increasing Δn. The phase-matching condition is irrelevant in this case.

ACKNOWLEDGMENTS

We thank K. M. Yoo for helpful discussions. One of the authors (V.E.K.) is grateful to the Alexander von Humboldt Foundation for the support during this work and to the Physical Department of Würzburg University for their hospitality.

*On leave from Institute of Spectroscopy, U.S.S.R. Academy of Sciences, 142092 Troitsk, Moscow r-n, U.S.S.R.

[1]P. A. Lee and T. V. Ramakrishnan, Rev. Mod. Phys. **57**, 287 (1985).

[2]V. I. Tatarski, *The Effect of a Turbulent Atmosphere on Wave Propagation* (National Technical Information Service, Washington, D.C., 1971).

[3]M. J. Stephen and G. Cwilich, Phys. Rev. Lett. **59**, 285 (1987).

[4]R. Berkovitz and M. Kaveh, Phys. Rev. B **36**, 9322 (1987).

[5]M. Rosenbluh, I. Edrei, M. Kaveh, and I. Freund, Phys. Rev. A **35**, 4458 (1987).

[6]S. Feng, C. Kane, P. A. Lee, and A. D. Stone, Phys. Rev. Lett. **61**, 834 (1988).

[7]F. C. MacKintosh and S. John, Phys. Rev. B **37**, 1884 (1988).

[8]M. B. van der Mark, M. P. van Albada, and A. Lagendijk, Phys. Rev. B **37**, 3575 (1988).

[9]E. Akkermans, P. E. Wolf, R. Maynard, and G. Maret, J. Phys. (Paris) **49**, 77 (1988).

[10]V. M. Agranovich and V. E. Kravtsov, Phys. Lett. A **131**, 378 (1988); **131**, 386 (1988); Zh. Eksp. Teor. Fiz. **95**, 484 (1989) [Sov. Phys. JETP **68**, 272 (1989)].

[11]V. E. Kravtsov, V. I. Yudson, and V. M. Agranovich, Phys. Rev. B **41**, 2794 (1990).

[12]A. Ishimaru, *Wave Propagation and Scattering in Random Media* (Academic, New York, 1978), Vol. 1.

[13]K. M. Yoo, S. Lee, Y. Takiguchi, and R. R. Alfano, Opt. Lett. **14**, 800 (1989).

[14]S. John, Phys. Rev. Lett. **53**, 2169 (1984).

[15]P. W. Anderson, Philos. Mag. B **52**, 505 (1985).

[16]M. Born and E. Wolf, *Principles of Optics* (Pergamon, New York, 1959).

[17]A. A. Abrikasov, P.L. Gor'kov, and I. E. Dzialoshinskii, *Methods of Quantum Field Theory in Statistical Physics* (Pergamon, New York, 1965).

[18]L. P. Gor'kov, A. I. Larkin, and D. E. Khmelnitskii, Zh. Eksp. Teor. Fiz. **30**, 248 (1979) [Sov. Phys. JETP Lett. **30**, 228 (1979)].

[19]A. I. Ekimov, Al. L. Efros, and A. A. Onuschenko, Solid State Commun. **56**, 921 (1988).

[20]R. K. Jain, and R. C. Lind, J. Opt. Soc. Am. **73**, 647 (1983).